NUMERICAL STUDY ON INFLUENCES OF FLOW DIVERSION ON CHANNEL MORPHOLOGY: CASE STUDY OF BAGMATI RIVER, CENTRAL NEPAL

Kapil Maharjan[*]
MEE19715

Supervisors: Prof. Shinji Egashira[**]
Dr. Atsuhiro Yorozuya[***]
Dr. Daisuke Harada[****]
Dr. Fumio Takeda[*****]

ABSTRACT

The study area is located in a transition zone between Mountain and the Terai Plain, where bank erosion due to the changing course of the Bagmati River is a major problem. To reduce bank erosion, this study proposed countermeasures to control flow patterns by means of levee embankments and investigated their effects using numerical simulations. The flow pattern and bed deformations were analyzed for different cases of bed load and suspended load to find an effective countermeasure. The numerical predictions suggested that the bed shear stress in the upstream reach increased spatially and temporarily compared to downstream, and that the increasing velocity in the left channel was a major factor enhancing bank erosion. The numerical results showed that one of the best countermeasures involved shifting the stream from the left to the right by means of an embankment.

Keywords: Flow diversion, Flow pattern, Morphological change, Bed deformation, Sediment transportation

INTRODUCTION

Bagmati River is a dynamic, spring-fed perennial river that originates from Shivapuri Mountain. The study area is located within a transition between the mountain and the Terai Plain. The basin is confined between two larger basins, the Gandaki Basin to the west and the Koshi Basin to the east. It stretches from 26°42′ and 27°50′N and 85°02′ and 85°58′E, and covers a total catchment area of 3750 km^2. The total length of the river, from its origin to the Nepal–India border, is 170 km. The annual mean discharge and annual mean peak discharge at Pandherodoban Hydrological Station are 138 m^3/s and 4876 m^3/s, respectively. The sudden fall of slope from the mountain to the plain changes the river reach geometry from narrow to wide, thereby causing excessive sedimentation. In addition, high-to-very high discharge and variation in altitude are the main factors influencing the morphological change. The Terai Plain is considered a depositional basin. Water- and sediment-related disasters are common due to extreme weather events, which trigger landslides, floods, slope failures, soil erosion, etc. Eventually, riverbed aggradation occurs, enhancing bank erosion and

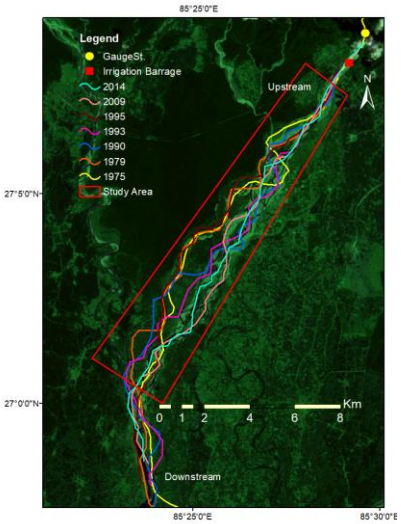

Figure 1: Change in the course of Bagmati River

[*] Hydrogeologist, Department of Water Resources and Irrigation, Nepal
[**] Professor, GRIPS, Tokyo and Research and Training Advisor, ICHARM, Tsukuba, Japan
[***] Associate Professor, GRIPS, Tokyo and Research and Training Advisor, ICHARM, Tsukuba, Japan
[****] Associate Professor, GRIPS, Tokyo and Research and Training Advisor, ICHARM, Tsukuba, Japan
[*****] Adjunct Professor, GRIPS, Tokyo

inundation. Figure 1 illustrates the study area as well as the annual changes in the course of the river. According to the results shown in this figure, such channel changes have occurred often over time. Given these active changes, erosion is common along the left bank. To provide countermeasures against excessive bank erosion of precious agricultural land, this study assesses the influences of flow diversion using numerical simulation with a two-dimensional depth-integrated model together with Nays2DH, a solver used to predict flow patterns, bed elevation, bed material size, and velocity with respect to depth.

METHODOLOGY

The numerical simulation was conducted with the depth-averaged mass and momentum conservation equations for water as well as the mass conservation equations for sediments as the governing equations, which are described below.

Continuity equation

$$\frac{\partial h}{\partial t}+\frac{\partial uh}{\partial x}+\frac{\partial vh}{\partial y}=0 \quad (1)$$

where h is the flow depth, t is the time, and u and v are the components of the depth-averaged flow velocities along the x and y directions, respectively.

Momentum conservation equations for describing the flow fields in the x and y directions

$$\frac{\partial uh}{\partial t}+\frac{\partial uuh}{\partial x}+\frac{\partial uvh}{\partial y}=-gh\frac{\partial H}{\partial x}-\frac{\tau_x}{\rho}+\frac{\partial h\sigma_{xx}}{\partial x}+\frac{\partial h\tau_{yx}}{\partial y} \quad (2)$$

$$\frac{\partial vh}{\partial t}+\frac{\partial uvh}{\partial x}+\frac{\partial vvh}{\partial y}=-gh\frac{\partial H}{\partial x}-\frac{\tau_y}{\rho}+\frac{\partial h\tau_{xy}}{\partial x}+\frac{\partial h\sigma_{yy}}{\partial y} \quad (3)$$

where u and v are the x and y components of the velocity near the bed surface,

Mass conservation equation for suspended sediment

$$\frac{\partial c_i h}{\partial t}+\frac{\partial r_{1u}c_i h}{\partial x}+\frac{\partial r_1 v c_i h}{\partial y}=\frac{\partial}{\partial x}\left(h\in_x\frac{\partial c_i}{\partial x}\right)+\frac{\partial}{\partial y}\left(h\in_y\frac{\partial c_i}{\partial y}\right)+E_i-D_i \quad (4)$$

where c, u, and v denote the depth-averaged values for the sediment concentration, x-component velocity, and y-component velocity, respectively. $\in_x$ and $\in_y$ are the x and y components of the dispersion coefficient (similar to the turbulent diffusion coefficient). E_i is the erosion rate of suspended sediment for grain size d_i . D_i is the deposition rate of the sediment for grain size d_i.

Mass conservation equation of bed sediment (equation of bed elevation)

$$\frac{\partial Z_b}{\partial t}+\frac{1}{1-\lambda}\sum_i\left(\frac{\partial q_{bix}}{\partial x}+\frac{\partial q_{biy}}{\partial y}+E_i-D_i\right)=0 \quad (5)$$

q_{bix} refers to the bedload transport rate in the x-direction for grain size d_i. q_{biy} is the bedload transport rate in the y-direction for grain size d_i. λ is the porosity of the bed sediment.

We employed Egashira et al.'s (1997b, 2005) formula for the bedload transport rate.

$$q_{b*}=\frac{4}{15}\frac{K_1K_2}{\sqrt{f_d+f_f}}\tau_*^{5/2} \quad (6)$$

Here, $K_1=\frac{1}{cos\theta}\frac{1}{tan\phi_s-tan\theta}$, $K_2=\frac{1}{c_s}\left[1-\frac{h_s}{h_t}\right]^{\frac{1}{2}}$, $f_d=k_d(1-e^2)(\frac{\sigma}{\rho})\bar{c}_s^{\frac{1}{3}}$, and $f_f=k_f(1-\bar{c}_s)^{\frac{5}{3}}\bar{c}_s^{\frac{-2}{3}}$,

where k_d takes the value 0.0828 (a universal constant), k_f equals 0.16 (a universal constant), ϕ_s or the internal friction angle equals 34–38 in natural sands, e takes the value 0.85 (a restriction), θ is the bed slope, σ is the mass density of a solid particle, ρ is the mass density of water, and $\bar{c}_s$ is the average sediment concentration of the bedload layer ($c_s=c_*/2$).

The erosion rate was evaluated using Itakura and Kishi's (1980) formula.

$$\frac{E}{u_*}=K\frac{w_0}{u_*}(\alpha_*\frac{\sigma-\rho}{\sigma}\frac{gd}{u_*w_0}\Omega-1) \quad (7)$$

where

$$\Omega=\frac{\tau_*}{B_*}\frac{\int_a^\infty{}'\xi\frac{1}{\pi}\exp(-\xi^2)d\xi}{\int_a^\infty{}'\frac{1}{\pi}\exp(-\xi^2)d\xi}+\frac{\tau_*}{B_*\eta_0}-1 \quad (8)$$

where w_0 denotes the fall velocity of the sediment particle. B_*, an empirical coefficient, takes the value 0.143. η_0, K, and α_*, all of which are empirical coefficients, equal 0.50, 0.008, and 0.14, respectively. The deposition rate is calculated as $D = w_0 c_b$, where c_b is the sediment concentration at the reference level over the bed surface, and $c_b = r\bar{c}$, where coefficient $r = {}^{c_b}/_{\bar{c}} \geq 1$.

This study was carried out according to the flow chart shown in Figure 2.

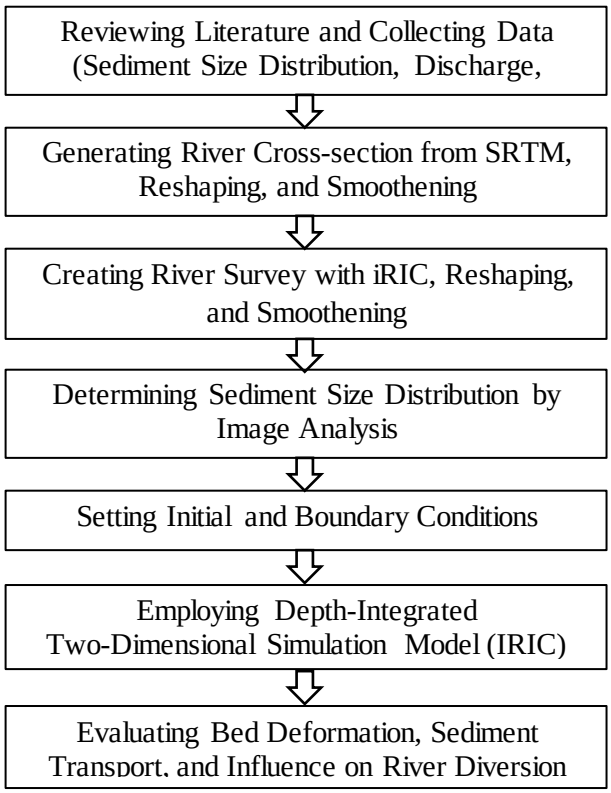

Figure 2: Methodology

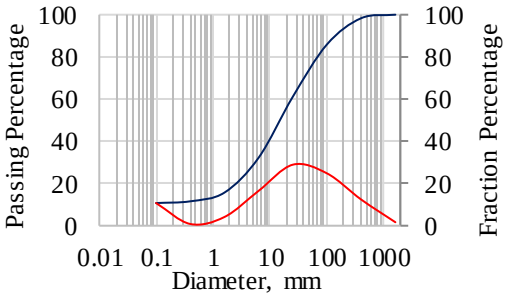

Figure 3: Particle size distribution of bed sediment

Figure 4: Pictures of bed material

DATA

The topographic data of 1 arcsec Shuttle Radar Topographic Mission (SRTM) Digital Elevation Model (DEM) of the study basin were downloaded from the USGS Earth Explorer website. The river cross-section was obtained with QGIS and SRTM, and smoothened with the help of Fourier transformation. The numerical simulation was conducted for a mean peak discharge of 5000 m^3/s under steady flow conditions. Non-uniform sediment with d_{50} as 17 mm was employed, as shown in Figures 3 and 4. Table 1 lists the computation conditions.

Table 1: Computation conditions for bed deformation.

S. No.	Description	Value/Applied Formula
1	Downstream and upstream slope values	0.0025
2	Manning's roughness coefficient (n)	0.03
3	Calculation time step (s)	0.5
4	Bed material type	Non-uniform
5	Sediment transport type	Bedload and suspended load
6	Minimum exchange layer thickness (m)	0.001
7	Bedload transport formula for non-uniform sediment	Egashira's (1997b, 2005) formula
8	Vector of bedload transport	Watanabe's (2001) formula
9	Upward flux of suspended load from the river bed	Itakura and Kishi's (1980) formula

RESULTS AND DISCUSSION

Figure 5 shows the flow pattern for a 30-d computation, in which stream bifurcation takes place upstream of the domain. The velocity is higher on the upstream side and in the left channel of the domain, which could enhance bank erosion in important agricultural land. Analyzing the results of the flow pattern showed that four different bed deformation cases could be conducted to evaluate the influences of flow diversion on channel morphology. The computational cases are illustrated in Table 2. All these cases were computed under a constant flow discharge of 5000 m^3/s. Case 1 was computed without an artificial structure, while Levees 1 and 2 were simulated in Case 2 to control flow bifurcation. Case 3 was computed with modified Levees 1 and 2, while Case 4 was simulated using Levee 1 only.

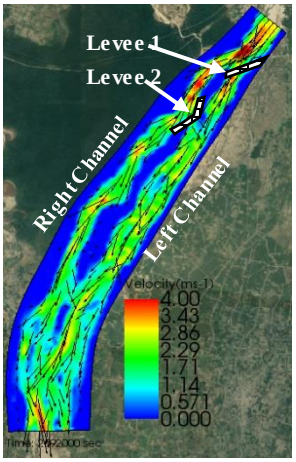

Figure 5: Flow pattern without bed deformation

Table 2: Computational cases.

Cases	Levee 1	Levee 1 (= 0.5H that of Case 1)	Levee 2	Remarks
1				Without structures
2				With Levees 1 and 2
3				With Levee 1 (= 0.5H that of Case 1) and Levee 2
4				With Levee 1
Note: H is a height of levee.				

Case 1: The results obtained for Case 1 are illustrated in Figures 6–9. Note that the computation was conducted for a time period of 30-d.

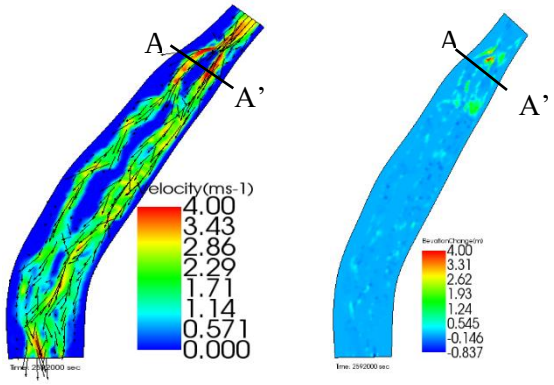

Figure 6: a) Velocity map and b) elevation change with bed deformation in Case 1

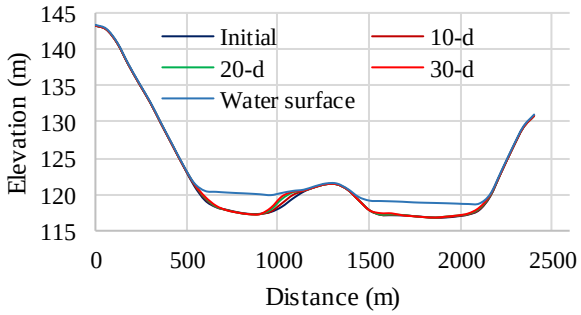

Figure 7: Cross-section at AA'

Figure 6(a) shows that the velocity in the left channel is sufficiently high to erode the bank. Figures 6(b) and 7 show that the bed elevation change occurs significantly upstream. Figure 8 illustrates that the bed shear stress in the upstream and downstream reaches increases spatially and temporarily over 10, 20, and 30-d of the computation. The bedload transport rate decreases due to sediment deposition on the upstream side and becomes nearly constant in the left channel with time, as shown in Figure 9. This computation also provides the discharge distribution in the right (34%) and left (60%) channels. Therefore, if we could reduce the flow discharge in the left channel, the problem posed by bank erosion on the left side could be solved. Such issues are discussed in Cases 2, 3, and 4.

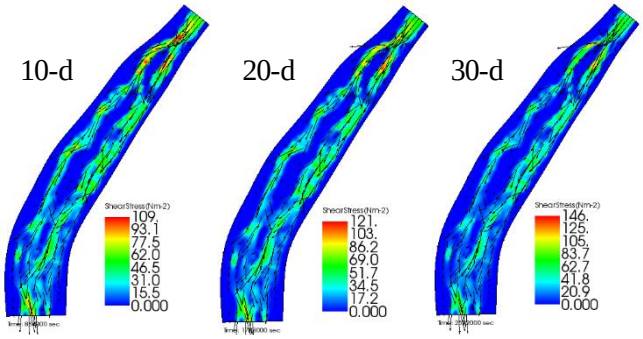

Figure 8: Temporal and spatial changes in shear stress

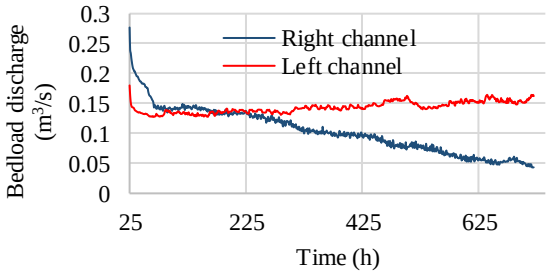

Figure 9: Bedload transport rate at AA'

Case 2: The results of Case 2 are illustrated in Figures 10–13. Figure 10(a) shows an elevation change that is active in comparison to that in Case 1. The velocity in the right channel, as shown in Figure 10(b), is very high, which could be attributed to channel clogging by sediment deposition on the left-hand side of the right channel, as shown at cross-section AA' in Figure 11.

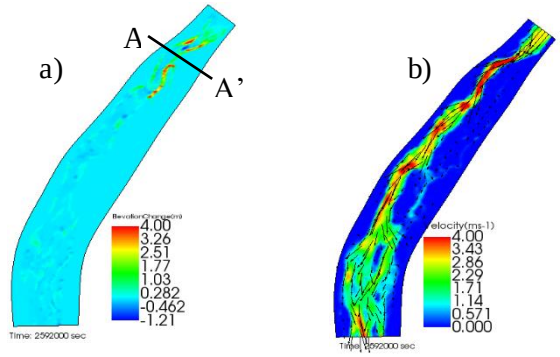

Figure 10: a) Elevation change and b) velocity map

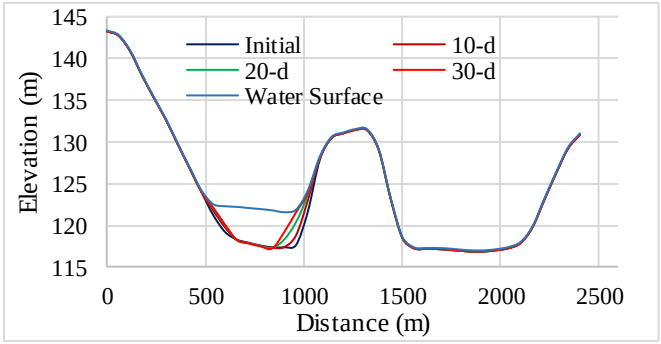

Figure 11: Cross-section at AA'

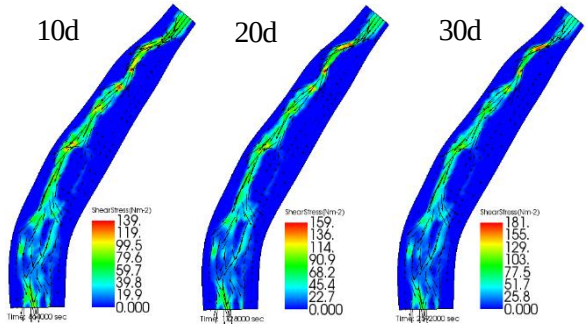

Figure 12: Temporal and spatial changes in shear stress

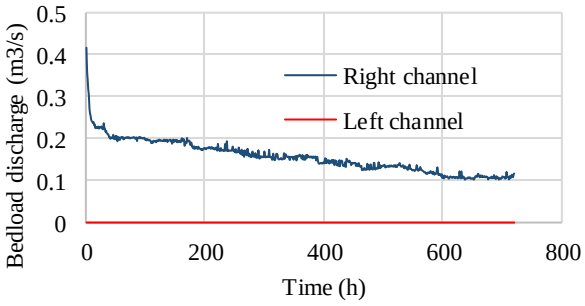

Figure 13: Bedload transport rate at AA'

Figure 12 shows the temporal and spatial distributions of bed shear stress, with the stress observed to be higher upstream than downstream. The impact of bed shear stress on the bedload transport rate at AA' is illustrated in Figure 13. It is observed that the bedload transport rate decreases continuously with respect to time.

Case 3: The results of Case 3 are shown in Figures 14–16. Figure 14 shows the depth-averaged two-dimensional velocity. The velocity in the left channel becomes very low in comparison to those of Cases 1 and 2. Figure 15 illustrates the temporal changes at cross-section AA'. The results show that channel narrowing occurs due to sediment deposition, resulting in high velocity in the right channel. Figure 16 shows that the bedload transport rate decreases in the right channel and is nearly constant in the left channel. At this stage, the flow discharge is estimated to be 77% in the right channel and 15% in the left channel.

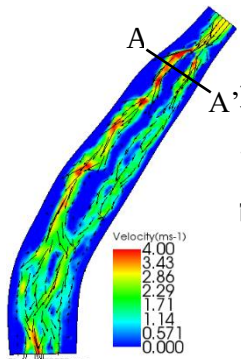

Figure 14: Velocity map

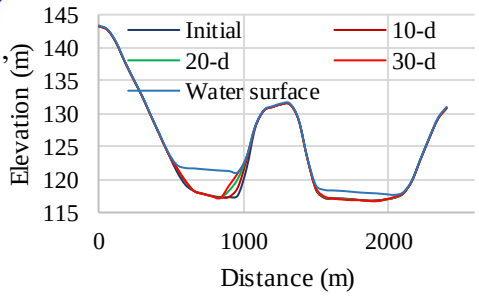

Figure 15: Cross-section at AA'

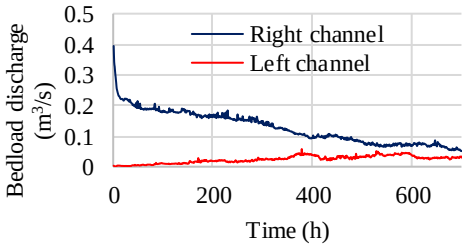

Figure 16: Bedload transport rate at AA'

Case 4: The results are illustrated in Figures 17–19. The sediment transport rate in the left channel to be negligible; thus, erosion does not occur so much along the left bank in this case as compare to other cases.

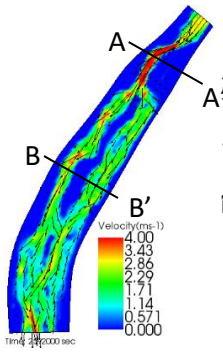

Figure 17: Velocity map

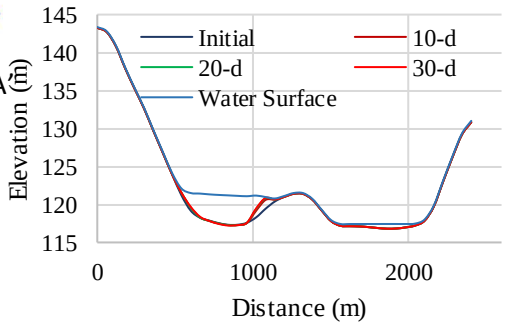

Figure 18: Cross-section at AA'

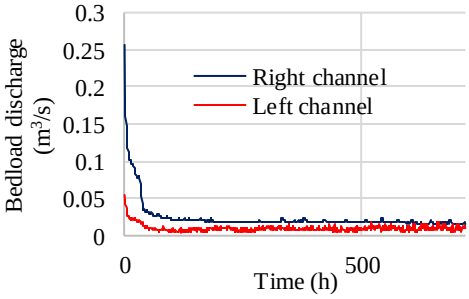

Figure 19: Bedload transport rate at BB'

CONCLUSIONS AND RECOMMENDATIONS

This study discussed countermeasures to decrease bank erosion along a specific section of the left bank by means of numerical simulations. The results suggested that Case 3, which involved modifications using Levee 1, could solve the existing problems in a manner superior to the spur and dyke method. However, a detailed investigation and survey are necessary to assess the effectiveness of the proposed structures in the field.

ACKNOWLEDGMENT

I would like to express my sincere gratitude to my supervisors, Professor Shinji Egashira, Dr. Atsuhiro Yorozuya (Associate Professor, ICHARM, PWRI), and Dr. Daisuke Harada (Research Specialist, ICHARM, PWRI) for their continuous support during my Master's degree program.

REFERENCES

Acharya, D. R. (2019). *Influence of sand bar behaviour of channel changes along Kaligandaki River, Nepal*. National Graduate Institute of Policy Studies (GRIPS), International Center for Water Hazard and Risk Management (ICHARM), Public Works Research Institute (PWRI). Available at: https://www.grips.ac.jp/cms/wp-content/uploads/2019/10/Synopsis_MEE18711Acharya.pdf. Accessed on August 7 2020.

Egashira, S. (2009-2020). *Mechanics of sediment transportation and channel changes, Manual for water Related Risk Management Course.*

Shrestha, P., & Tamrakar, N. K. (2012). *Morphology and classification of the main stem Bagmati River, Central Nepal*. Bulletin of the Department of Geology. Vol. 15, pp. 23–34

Watanabe, A., Fukuoka, S., Yasutake, Y. and Kawaguchi, H. (2001). *Method for Arranging Vegetation Groins at Bends for Control of Bed Variation*, Advances on River Engineering, 7, 285-290.

Yasuyuki, S., & Takebayashi, H. (2014). iRIC software, ver. 3.2, Nays2DH Solver Manual.